American Mineralogist, Volume 90, pages 448–456, 2005

Ordering and elasticity associated with low-temperature phase transitions in lawsonite

P. SONDERGELD,[1,5,*] W. SCHRANZ,[1] A. TRÖSTER,[1] T. ARMBRUSTER,[2] G. GIESTER,[3] A. KITYK,[4] AND M.A. CARPENTER[5]

[1]Institut für Experimentalphysik, Universität Wien, Strudlhofgasse 4, A-1090 Wien, Austria
[2]Laboratorium für chemische und mineralogische Kristallographie, Universität Bern, Freiestrasse 3, CH-3012 Bern, Switzerland
[3]Institut für Mineralogie und Kristallographie, Universität Wien, Althanstrasse 14, A-1090 Wien, Austria
[4]Institute for Computer Science, Faculty of Electrical Engineering, Technical University of Czestochowa, Armii Krajowej 17, 42-200 Czestochowa, Poland
[5]Department of Earth Sciences, University of Cambridge, Downing Street, Cambridge CB2 3EQ, U.K.

ABSTRACT

The two low-temperature phase transitions of lawsonite have been studied using single-crystal X-ray diffraction from 86 to 318 K and a single-crystal high-frequency continuous-wave resonance technique from 323 to 102 K. While recently published data of the variations of strains, birefringence, and IR line widths are consistent with the (271 K) *Cmcm-Pmcn* transition being simply tricritical, our investigation of critical X-ray reflections and the six diagonal elastic constants of lawsonite reveals, consistently, a more complex crossover pattern in the temperature range of 205–225 K. Below 205 K the overall pattern is again in good agreement with a tricritical solution of the *Cmcm-Pmcn* transition and a second-order behavior of the (120 K) *Pmcn-P*2_1*cn* transition. The structure determination from single-crystal X-ray data at 215 K reveals a possible orientational disorder of some of the hydroxyl groups in the *Pmcn* phase. From this and a recent strain analysis of deuterated and hydrogenated lawsonite we conclude that down to 205 K the *Cmcm-Pmcn* transition is driven by a displacive component, as observed in strain and birefringence data, plus an order/disorder component or dynamical effects associated with proton ordering. Below 205 K only the displacive component plays a role, and the (120 K) *Pmcn-P*2_1*cn* transition is driven by a single order parameter. The remarkable elastic softening of C_{66} ahead of the *Cmcm-Pmcn* transition indicates another orthorhombic-monoclinic transition, which is suppressed on cooling through the low-temperature phase sequence *Cmcm-Pmcn-P*2_1*cn*, but can be observed on applying pressure to the mineral.

INTRODUCTION

Lawsonite, $CaAl_2[Si_2O_7](OH)_2 \cdot H_2O$, is seen as an essential component in the geological water cycle (Pawley 1994) due to the high water content of ~11 wt% and the occurrence in high-pressure, low-temperature metamorphic environments. Figure 1 shows the room-temperature structure of lawsonite at ambient pressure. The framework consists of infinite linear chains of $[AlO_6]$ octahedra bridged via $[Si_2O_7]$ building blocks. The cavities are occupied by Ca^{2+} ions, water molecules, and hydroxyl groups. The polymorphism of lawsonite has attracted considerable interest over the last few years. To date five different phases of lawsonite are known with two low-temperature phase transitions around ~271 K (T_1) and ~120 K (T_2) at ambient pressure and two high-pressure phase transitions around ~4 and ~9.5 GPa at room temperature (Daniel et al. 2000; Boffa Ballaran and Angel 2003). Libowitzky and Armbruster (1995) have determined the structures of both the room-temperature phase and the two low-temperature phases. These differ from one another mainly with respect to the arrangement of the hydrogen-bearing components and thus the hydrogen bond system. Both low-temperature phase transitions are accompanied by changes of the special-site symmetry of the water molecules, and the one at lower temperature (T_2) also affects the special-site symmetry of the hydroxyl groups. The authors deduce that the water molecules are dynamically disordered at room temperature. It follows that the two phase transitions involve ordering processes of the water molecules. The hydroxyl groups are affected by this via the hydrogen bond system. In addition, neutron diffraction experiments have shown that some of the hydroxyl groups remain disordered at 20 K (Lager et al. 1998).

A closer inspection of the ordering processes has recently been initiated (Meyer et al. 2000, 2001; Sondergeld et al. 2000a, 2000b; Carpenter et al. 2003), involving studies of the temperature dependence of physical properties such as birefringence, lattice parameters, and IR line widths that are correlated with the macroscopic order parameters. All these data are consistent with a rather simple tricritical *Cmcm-Pmcn* transition, while the *Pmcn-P*2_1*cn* transition associated with T_2 appears to be second order.

Nevertheless, the birefringence data and recent calorimetric studies (Martín-Olalla et al. 2001), in particular, indicate signifi-

* E-mail: Peter.Sondergeld@esc.cam.ac.uk

0003-004X/05/0203–448$05.00/DOI: 10.2138/am.2005.1243

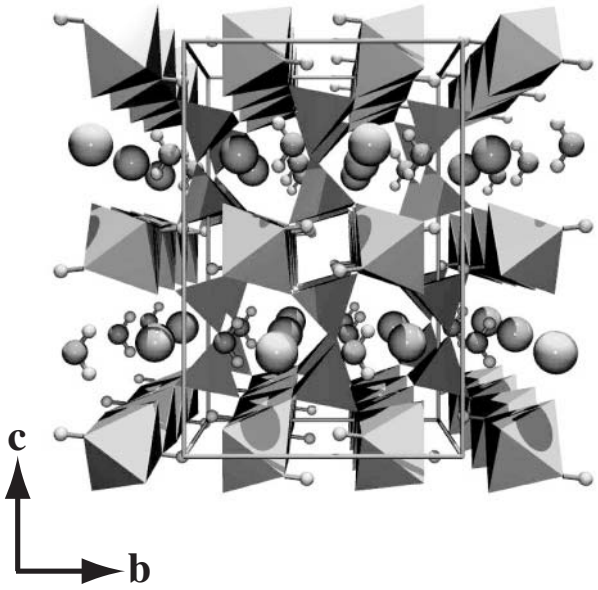

FIGURE 1. The room-temperature structure of lawsonite (space group *Cmcm*) projected along [100], with infinite linear chains of edge-connected [AlO_6] octahedra along [100] that are bridged via [Si_2O_7] building blocks. In the cavities are Ca^{2+} ions, H_2O molecules, and OH groups.

cant pretransitional effects ahead of the *Cmcm-Pmcn* transition. In addition, it turns out that the variation of the specific heat with temperature depends strongly on the direction of the experiment. While on heating the variation of the specific heat is consistent with a tricritical phase transition, the pattern is quite different on cooling and a significant hysteresis is observed, contrary to the strain, birefringence, and IR data. The unusual behavior on cooling is attributed to kinetic effects (Hayward et al. 2002) that could possibly be avoided by using a very slow cooling rate. The elastic constants are correlated with the heat capacity. Both kinds of properties are obtained from second derivatives of the free energy and are therefore explicitly sensitive to the order-disorder phase transitions discussed here. Schilling et al. (2003) recently studied the temperature dependence of all nine elastic constants of lawsonite in the *Cmcm* phase using Brillouin spectroscopy in the temperature range 294–723 K.

Little is known about the effect of the two low-temperature phase transitions on the elastic properties of lawsonite. Three Young's moduli have been studied in the temperature range 88–350 K using the low-frequency DMA technique (Sondergeld et al. 2000a, 2000b). Although these data give a limited description of the elastic behavior of lawsonite at low temperatures, they do not give the individual elastic constants. One method for studying elastic constants is the single-crystal high-frequency continuous-wave resonance technique, which was used in this study to obtain the temperature dependence of the six diagonal components of the elastic stiffness tensor at low temperatures.

On cooling below room temperature, the structure of lawsonite is characterized by a compression of the unit-cell volume which is barely influenced by the two low-temperature phase transitions (Sondergeld et al. 2000a; Carpenter et al. 2003). The closer packing in the **bc** plane is compensated by an expansion along the basis vector **a**. In hennomartinite, the SrMn-analogue to lawsonite (Ca and Al are replaced by Sr and Mn, respectively), the same phase sequence is observed on heating (Libowitzky and Armbruster 1996), although the transition points are at higher temperatures. On subsequent cooling, however, a *Cmcm* – ($T_1 \approx 423$ *K*) → *Pmcn* transition and a monoclinic phase were observed below $T_m \approx 368$ K. The lattice relations between the *Cmcm* phase and the two high-pressure phases of lawsonite (Daniel et al. 2000; Boffa Ballaran and Angel 2003) are consistent with the phase sequence obtained on cooling hennomartinite. The influence of the monoclinic distortion of the *Pmcn* structure involving the angle γ, as observed on cooling hennomartinite or applying pressure to lawsonite, would be directly linked to the elastic constant C_{66}.

Carpenter et al. (2003) made a detailed strain analysis of deuterated and hydrogenated lawsonite and predicted the behavior of the elastic constants, based on a displacive model of the two low-temperature phase transitions. Although they observed very subtle anomalies around ~225 K in the strain data for natural lawsonite, the strain, birefringence, and IR data are all consistent with a nearly tricritical phase transition at ~271 K (*Cmcm-Pmcn*) driven by a single order parameter. The data presented in this study, i.e., the temperature dependence of the intensities of critical X-ray reflections and the six diagonal elastic constants, suggest that the *Cmcm-Pmcn* transition is actually more complex and that previous studies have essentially captured only the displacive component involved in the transition.

EXPERIMENTAL SETUP

Samples

The lawsonite crystals used in this study were cut from lawsonite veins in blueschist rocks from the type locality at Tiburon Peninsula, Marin County, California, U.S.A. The X-ray data collection at 215 K and the X-ray intensity study were done using two different pieces from sample no. A7331 of the Natural History Museum, Bern, while the elastic measurements were done using a crystal cut from sample no. G14555 of the South Australian Museum in Adelaide, Australia.

X-ray diffraction

Temperature dependence of intensities. A single-crystal fragment of lawsonite (diameter: ~0.25 mm) was examined on an Enraf-Nonius CAD4 four-circle diffractometer using Mo$K\alpha$ radiation. The temperature around the crystal was controlled using a commercial cooling device with an open nitrogen gas flow and a Cu-CuNi thermocouple in the vicinity of the sample. The temperature calibration procedure included two absolute reference points at 77 and 295 K, respectively.

The measured reflections were subdivided into four different categories: 10 of the strongest reflections (type **A**) were used to check the change of the crystal with temperature and time, independent of the ordering behavior. Ten of the strongest reflections fulfilling the condition $h + k = 2n + 1$ (type **B**) were chosen to study the ordering associated with T_1. Since no additional extinction rules are connected with the ordering associated with T_2, 11 of the strongest reflections were chosen (type **C**) with little or no intensity above T_2 and a significant intensity below the transition point to follow this transition. Fourteen reflections, broadly distributed through reciprocal space, were used to determine the orienting matrix of the crystal (type **D**). At each temperature of interest, the orientation matrix was redetermined first, then the intensities and profiles (ω-scans) of the reflections of types **A**, **B**, and **C** were measured. The data collection was done stepwise, starting at 86 K and continuing in 4° steps up to 158 K, then in 8° steps up to 318 K, with an average temperature fluctuation of ±2°. The intensities of the type **A** reflections were practically constant over the whole temperature range examined. On heating from 86 K to 318 K, an average decrease of only 3% was observed. Therefore the intensities of reflections

of types **B** and **C** did not have to be corrected with respect to the reflections of type **A**. Initially, the temperature dependences of the intensities of all reflections of types **B** and **C** and the squares of the intensities of the reflections of type **B** were studied individually. While the intensities vary a little with respect to the behavior in the vicinity of the transition point, the overall pattern further away from this point is the same. Since the measurements were not designed to study fluctuations, but to examine the mean-field behavior further away from the transition point, we concluded that averaging the intensities of a certain type is justified to find out more about the character of the transition (tricritical, second-order, etc.) and actually very useful to improve the statistics, provided that the overall pattern of behavior is the same. Therefore the intensities of 10 of the strongest reflections of type **B** and 9 of the strongest reflections of type **C** were averaged, using a weighting scheme that favors intensities with a good I:σ(I) ratio, and normalized. In order to ensure a random contribution to the average intensity, only symmetrically independent ("unique") reflections were chosen for the averaging procedure. Table 1 lists the selected reflections along with their intensities at 86 K. Typically, the value of the intensity of an individual superlattice/critical reflection should be highest at the lower limit of the accessible temperature range (86–318 K) of the data collection. Due to the poorer I:σ(I) ratio, weaker reflections than those given in Table 1 would not significantly contribute to or improve the averaged and normalized intensity. A linear fit to the curve of the square of the reduced type **B** intensity gives a transition temperature of $T_1 \approx 270$ K, while another linear fit to the curve of the reduced type **C** intensity gives a transition temperature of $T_2 \approx 123$ K.

Structure determination at 215 K. A single-crystal fragment of lawsonite (diameter: ~0.15 mm) was selected and put on a Nonius Kappa single-crystal X-ray diffractometer with a CCD area detector. The crystal was cooled down to 215 K in the cold nitrogen gas flow of an Oxford Cryostream Cooler. While maintaining this temperature, a complete X-ray data collection (Mo$K\alpha$ radiation) was performed to determine the low-temperature crystal structure of lawsonite at 215 K. Then, from the reduced data, a structure refinement was done using the program package Shelx-97 (Sheldrick 1997). Details of the data collection and structure refinement are given in Table 2.

Elastic measurements

A single-crystal fragment of lawsonite was cut to a cube-shaped crystal and polished, with faces perpendicular to the main crystallographic directions of the orthorhombic phases ($a \times b \times c = 2.692 \times 2.552 \times 2.615$ mm^3). The temperature dependence of six components of the elastic stiffness tensor of lawsonite was determined using the continuous-wave resonance technique in the MHz region (Bolef and Menes 1960). This technique is based on the generation of standing waves in the crystal with the propagation direction parallel to a main crystallographic direction. In order to determine C_{11}, C_{22}, and C_{33}, longitudinal waves were generated propagating along [100], [010], and [001], respectively. In the cases of C_{44}, C_{55}, and C_{66}, transverse waves were generated propagating along [010], [100], and [100], with polarization directions along [001], [001], and [010], respectively. The transducer material was lithium niobate with resonance frequencies of 15 MHz (longitudinal) and 13 MHz (transverse). The crystal was attached to the transducer via a thin film of glycerol (86–273 K) and glucose (273–323 K). The sample was cooled down stepwise from 323 to 86 K over a period of 12 hours, corresponding to an average cooling rate of 20 Kh^{-1}. At each temperature step, the frequency dependence of the impedance of the composite oscillator (transducer + coupling film + sample) was recorded in the range 6–13 MHz using an HP 4192A LF impedance analyzer. The positions of the resonance peaks of the composite oscillator were determined and recalculated into those of the pure sample by applying the correction

$$\nu_{S,n} = \nu_{C,n} - \frac{\rho_T l_T}{\rho_S l_S}(\nu_T - \nu_{C,n}) \quad (1)$$

after Bolef and Menes (1960), where $\nu_{S,n}$ and $\nu_{C,n}$ represent, respectively, the specimen and composite oscillator resonance frequencies corresponding to the nth mechanical resonance (ρ = density, l = thickness, T = transducer, S = sample). The phase velocity v of the standing wave was calculated via the relation $v = 2 l_S \nu_{S,n}/n$ and recalculated into the respective elastic constant C_{ii} ($i = 1 – 6$) via the Christoffel Equation, i.e., $C_{ii} = \rho_S \cdot v^2$. The temperature calibration of the Ni-NiCr thermo-element in the vicinity of the sample included two absolute reference points, namely the transition temperatures of pure $KMnF_3$ at 91 and 186.7 K (Gibaud et al. 1991).

Table 1. Indices and single-crystal X-ray intensities (at 86 K) of type **B** and **C** reflections, used for determining the averaged and normalized intensity associated with the *Cmcm-Pmcn* transition (I_B) and the *Pmcn-P*2$_1$*cn* transition (I_C), respectively

Type **B**		Type **C**	
$h\,k\,l$	Intensity	$h\,k\,l$	Intensity
0 1 7	1190(35)	6 $\bar{2}$ 1	538(23)
0 1 12	489(22)	5 $\bar{5}$ 5	449(21)
2 5 8	469(22)	9 $\bar{5}$ 0	139(12)
2 5 3	448(21)	9 $\bar{1}$ 9	135(12)
2 7 10	338(18)	8 $\bar{6}$ 8	127(11)
0 3 14	335(18)	7 $\bar{7}$ 7	101(10)
0 1 5	309(18)	4 $\bar{2}$ 19	77(9)
2 3 4	290(14)	8 $\bar{2}$ 14	56(7)
1 2 17	246(16)	5 $\bar{7}$ $\bar{17}$	55(7)
3 6 14	230(15)		

Landau theory

Recently published data of the variations of strains, birefringence, and IR line widths of natural lawsonite (Meyer et al. 2000, 2001; Sondergeld et al. 2000a, 2000b) indicate a simple tricritical *Cmcm-Pmcn* transition driven by a single order parameter. An appropriate Landau expansion for this case is (Carpenter et al. 2003)

$$G = \frac{1}{2}a\Theta_s\left[\coth\left(\frac{\Theta_s}{T}\right) - \coth\left(\frac{\Theta_s}{T_c}\right)\right]Q^2 + \frac{1}{4}bQ^4 + \frac{1}{6}cQ^6 + \lambda_1 e_1 Q^2 + \lambda_2 e_2 Q^2 + \lambda_3 e_3 Q^2 + \lambda_4 e_4^2 Q^2 + \lambda_5 e_5^2 Q^2 + \lambda_6 e_6^2 Q^2 + \frac{1}{2}\sum_{i,k} C_{ik}^{\circ} e_i e_k \quad (2)$$

where Q is the order parameter, a, b, c, are normal Landau coefficients, T_c is a critical temperature, λ_1-λ_6 are strain/order parameter coupling coefficients, e_1–e_6 are components of the spontaneous

Table 2. Experimental details of the X-ray data collection of lawsonite at 215 K and subsequent structure refinement of the *Pmcn* phase

Experimental conditions	
Temperature (K)	215
Wavelength (Å)	0.71069 (Mo$K\alpha$)
θ range	$2.79 \le \theta \le 36.20$
Index ranges	$-9 \le h \le 9$
	$-14 \le k \le 14$
	$-21 \le l \le 21$
Crystal data	
Crystal diameter (mm)	0.15
μ (cm^{-1})	16.0
ρ_{cal} (g cm^{-3})	3.10
Formula units, Z	4
Space group	*Pmcn* (no. 62)
Lattice parameters:	
a (Å)	5.8515(3)
b (Å)	8.7768(4)
c (Å)	13.1107(6)
V (Å^3)	673.332(6)
Structure refinement	
Reflections:	
All	3275
Unique	1751
Unique, $I > 2\sigma(I)$	1290
R_{int}	0.0135
R_σ	0.0252
Final R ($I > 2\sigma(I)$):	
R_1	0.0226
wR_2	0.0693
Final R (all data):	
R_1	0.0322
wR_2	0.0744
Goodness of fit on F^2	1.100

strain, and C^0_{ik} are the elastic constants of the high-symmetry phase, in this context those of the *Cmcm* phase. The behavior of the strains e_1–e_6 can easily be deduced from this equation. In general, the strains are functions of the order parameter, the coupling coefficients, and the "bare" elastic constants C^0_{ik}. The term $\Theta_s\left[\coth\left(\frac{\Theta_s}{T}\right)-\coth\left(\frac{\Theta_s}{T_c}\right)\right]$ considers the leveling off or "saturation" of the order parameter at low temperatures. Θ_s is the saturation temperature.

Equation 2 can be renormalized to

$$G=\frac{1}{2}a\Theta_s\left[\coth\left(\frac{\Theta_s}{T}\right)-\coth\left(\frac{\Theta_s}{T_c}\right)\right]Q^2+\frac{1}{4}b^*Q^4+\frac{1}{6}cQ^6 \quad (3)$$

where b^* is a function of the coupling coefficients and the bare elastic constants.

Variations of the elastic constants can be deduced as (Slonczewski and Thomas 1970)

$$C_{ik}=C^0_{ik}-4\lambda_i\lambda_kQ^2\chi \qquad (i,k=1,2,3) \quad (4)$$

and

$$C_{ii}=C^0_{ii}+2\lambda_iQ^2 \qquad (i=4,5,6) \quad (5)$$

where χ is the order parameter susceptibility. It is related to the order parameter via the expression

$$\chi^{-1}=a\Theta_s\left[\coth\left(\frac{\Theta_s}{T}\right)-\coth\left(\frac{\Theta_s}{T_c}\right)\right]+(2b+b^*)Q^2+5cQ^4. \quad (6)$$

Since the strain, birefringence, and IR data of lawsonite indicate a second-order *Pmcn*-$P2_1cn$ transition driven by a single order parameter, Equations 2–6 can be applied to this transition as well. The parameters and coefficients are, of course, different. C^0_{ik}, in particular, represent the elastic constants of the *Pmcn* phase.

For a tricritical transition, $b^*=0$ and the temperature dependence of the order parameter is given by

$$Q^4=\frac{a\Theta_s}{c}\left[\coth\left(\frac{\Theta_s}{T_c}\right)-\coth\left(\frac{\Theta_s}{T}\right)\right] \quad (7)$$

For a second-order transition, $c=0$ and the solution is

$$Q^2=\frac{a\Theta_s}{b^*}\left[\coth\left(\frac{\Theta_s}{T_c}\right)-\coth\left(\frac{\Theta_s}{T}\right)\right] \quad (8)$$

Experimental results

X-ray diffraction

Temperature dependence of intensities. Libowitzky and Armbruster (1995) showed that the *Cmcm-Pmcn* phase transition of lawsonite at T_1 is essentially characterized by the order-disorder behavior of the water molecules. Above T_1 the molecules jump between two slightly different orientations, resulting in a special-site symmetry *m*2*m* for the dynamically disordered molecule. Cooling down through T_1 results in a preference for one of the two possible orientations. With regard to the orthorhombic lattice, which is common to both phases involved, the microscopic one-component order parameter Q_1 of this transition can thus be described as an effective rotation of the water molecule around [100]. In addition, the *Cmcm-Pmcn* transition involves a reduction of the Bravais lattice symmetry. Reflections fulfilling the condition $h+k=2n+1$ (type **B**) have, by definition, zero intensities above T_1, while the intensity below T_1 is proportional to the square of the order parameter Q_1. The same is true for the relation between the purely non-symmetry-breaking strain e_i ($i=1-3$) and the order parameter Q_1, implying that e_i^2 is proportional to ${Q_1}^4$.

Figure 2 shows the temperature dependence of the square of the strain e_2 of natural (hydrogenated) lawsonite (Sondergeld et al. 2000a, 2000b). The linear temperature dependence of e_2^2 in the range T_1-T_2 is a typical example of tricritical behavior, as described by Equation 7. Carpenter et al. (2003) have estimated a Θ_s of 125(7) K for the order parameter of the *Cmcm-Pmcn* transition, implying saturation effects below ~65 K and a nearly linear relationship $Q_1^4 \propto |T_1-T|$ between T_1 and 86 K, the lower limit in this study. These findings are consistent with temperature variations of birefringence and IR line widths (Meyer et al. 2000).

A tricritical behavior would also imply $I_B^2 \propto Q_1^4 \propto |T_1-T|$ for the temperature range T_1-T_2, where I_B represents the intensity of a type **B** superlattice reflection. Contrary to expectations this is not the case. None of the intensities of the individual type **B** reflections shows the predicted behavior. Instead, the various intensities show a uniform pattern, which was statistically improved and reduced to a single averaged and normalized intensity (cf. the Experimental Setup section for further details). Figure 3 shows a plot of the square of the thus reduced type **B** intensity vs. temperature. Contrary to expectations for tricritical behavior, there appear to be two linear sections in the data (instead of just one), as indicated by the fitted solid and dashed lines, with a change in slope at ~222 K. There are not enough data points between T_1 and 222 K to clarify whether the *Cmcm-Pmcn* transition behaves tricritically in this range or gradually changes according to a more complicated mechanism. Below 222 K, however, the pattern looks tricritical again, though it cannot be extrapolated to

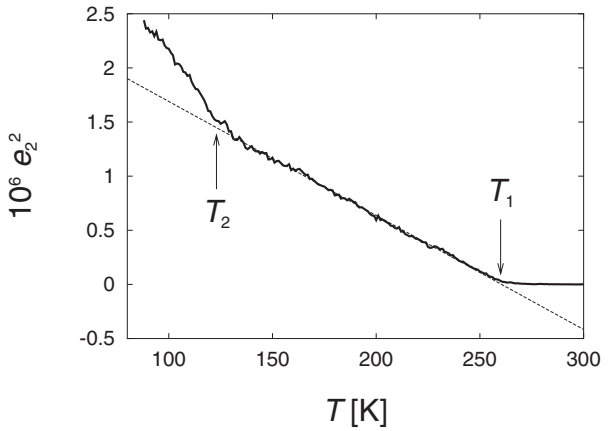

Figure 2. Square of the strain e_2 vs. temperature, where $e_2=(b-b_0)/b_0$ refers to the *Cmcm-Pmcn* transition associated with T_1. The symbol b describes the lattice parameter variation in the *Pmcn* phase, while b_0 refers to the extrapolated variation in the higher-symmetry *Cmcm* phase under the same conditions. The variable e_2^2 varies linearly with temperature, i.e., shows tricritical behavior between T_1 and T_2.

the original transition temperature at $T_1 \approx 270$ K. In other words, the conditions below 222 K are not a simple continuation of a tricritical *Cmcm-Pmcn* transition starting at T_1.

The *Pmcn-P*2_1*cn* transition associated with T_2 is characterized by reorientations of both the water molecules and the hydroxyl groups (Libowitzky and Armbruster 1995) out of the **bc** plane, thus reducing the special-site symmetry of the hydrogen-bearing components from *m* to 1. Intensities of reflections of type **C** are proportional to the square of the order parameter Q_2 associated with T_2. The intensities of critical type **C** reflections show a uniform pattern below T_2. Carpenter et al. (2003) estimated a Θ_s of 135(35) K for the order parameter Q_2 of the *Pmcn-P*2_1*cn* transition. The uncertainty of the saturation temperature is high. Nevertheless, saturation effects are not expected between T_2 and 86 K, so that a relationship $I_C \propto Q_2^2 \propto |T_2 - T|$ is predicted according to Equation 8 within the range $T_2 - 86$ K. Again, instead of presenting all type **C** reflections individually, they have been statistically improved and reduced to a single averaged and normalized intensity (see the Experimental Setup section). Figure 4 shows the variation of the thus reduced intensity I_C with temperature. It clearly varies linearly with temperature between T_2 and 86 K. Thus, contrary to the intensities of type **B** reflections

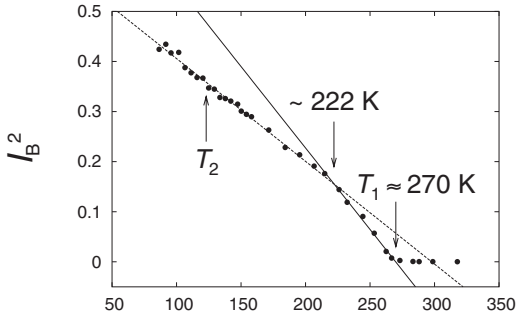

FIGURE 3. Square of the intensity I_B vs. temperature, where I_B is the averaged and normalized intensity of 10 unique single-crystal X-ray superlattice reflections associated with the *Cmcm-Pmcn* transition around T_1. Contrary to expectations of tricritical behavior, there appear to be two linear sections in the data (instead of just one), as indicated by the fitted solid and dashed lines, with a change in slope at ~222 K.

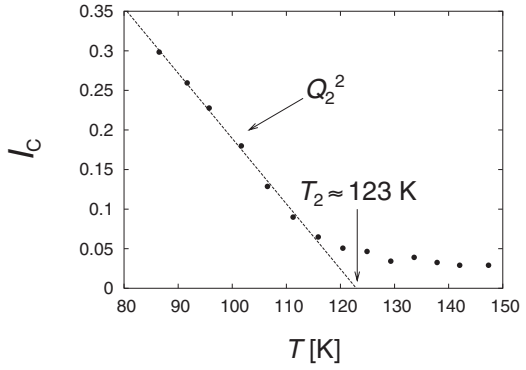

FIGURE 4. Temperature dependence of the averaged and normalized intensity I_C of nine unique critical single-crystal X-ray reflections associated with the *Pmcn-P*2_1*cn* transition around T_2. As expected, I_C varies linearly with temperature, which is consistent with a classical second-order transition.

associated with the *Cmcm-Pmcn* transition, the intensities of type **C** reflections behave in full agreement with recently published strain, birefringence, and IR data (Meyer et al. 2000, 2001; Sondergeld et al. 2000a, b), with better statistics, thus supporting the assumption that the *Pmcn-P*2_1*cn* transition is driven by a single order parameter and is second order.

Structure determination at 215 K. The crossover behavior of the type **B** X-ray reflections implies, among other things, subtle changes of the crystal structure of natural (hydrogenated) lawsonite around 222 K. Table 3 gives the results of the structure determination from X-ray data at 215 K, i.e., just below this temperature. It lists the fractional co-ordinates and isotropic displacement parameters of all atoms of the asymmetric unit. Except for the hydrogen atoms, all atoms were refined anisotropically. As expected, the fractional co-ordinates of the framework atoms—Ca, Al, Ala, Si, Sia, O1, O2, O2a, O3, and O3a—are very close to their respective positions in the higher-symmetry *Cmcm* phase at 295 K (Libowitzky and Armbruster 1995), while the atoms of the hydrogen-bearing components have changed their positions significantly. Their new positions can be seen essentially as the result of rotations in the **bc** plane, with rotation axes parallel to [100]. The water molecules are rotated by ~20° and the bonds of the hydroxyl groups by ~17° (O4-Hh) and ~28° (O4a-Hha), respectively, relative to the structure at 295 K. Table 4

TABLE 3. Unique sites and equivalent isotropic displacement parameters of the atoms of the asymmetric unit of the *Pmcn* phase of lawsonite at 215 K

Atom	*x*	*y*	*z*	U_{eq}
Ca	0	0.33243(1)	0.25072(1)	0.00745(2)
Al	1/4	1/4	0	0.00413(3)
Ala	1/4	1/4	1/2	0.00383(3)
Si	0	0.98045(1)	0.13204(1)	0.00417(2)
Sia	0	0.97888(1)	0.36585(1)	0.00416(2)
O1	0	0.04971(4)	0.24903(2)	0.00699(6)
O2	0.27482(4)	0.37460(2)	0.11933(1)	0.00705(4)
O2a	0.27177(4)	0.37994(2)	0.38419(1)	0.00608(4)
O3	0	0.13736(3)	0.06351(2)	0.00562(6)
O3a	0	0.13592(3)	0.43419(2)	0.00576(6)
O4	0	0.64019(3)	0.05069(2)	0.00593(6)
O4a	0	0.63476(4)	0.45762(2)	0.00739(7)
O5	0	0.60880(5)	0.24857(2)	0.01533(9)
Hw	0	0.6420(8)	0.1849(6)	0.037(2)
Hwa	0	0.681(1)	0.2870(7)	0.046(2)
Hh	0	0.5395(9)	0.0386(6)	0.047(2)
Hha	0	0.5638(14)	0.4245(9)	0.104(4)

Note: All atoms, except the hydrogen atoms, were refined anisotropically.

TABLE 4. Distances < 3 Å between the hydrogen and oxygen atoms in the structure of the *Pmcn* phase of lawsonite at 215 K

Pair	Distance
Hw-O5	0.884(7)
Hw-O4	1.760(7)
Hw-O2a	2.640(6)
Hwa-O5	0.810(9)
Hwa-O4a	2.274(9)
Hwa-O2	2.476(7)
Hh-O4	0.898(8)
Hh-O4a	1.861(8)
Hh-O2	2.409(6)
Hh-O2a	2.669(7)
Hha-O4a	0.76(1)
Hha-O2a	2.327(9)
Hha-O5	2.34(1)
Hha-O4	2.44(1)

gives all distances < 3 Å between H and O atoms in the structure. The water molecule consists of the atoms Hw, O5, and Hwa. The Hw-O5-Hwa bond angle of 109.2(8)° is larger and the Hw-O5 and Hwa-O5 bond lengths smaller than those of the free molecule (O-H bond length: 0.98 Å, H-O-H bond angle: 104.5°). These are still realistic, taking into account the librational motion of the molecule, the restraints due to hydrogen bonds, and the error caused by the localization of the atomic positions from electron densities. The *Cmcm-Pmcn* transition involves a splitting of the O and H positions of the hydroxyl groups into two symmetrically independent groups (O4-Hh and O4a-Hha). Again, the O-H bond lengths of the hydroxyl groups at 215 K are realistic. The four H positions of the asymmetric unit do not only form covalent O-H bonds; Table 4 shows that Hw and Hh additionally form hydrogen bonds with distances of less than 1.9 Å. All other O-H distances are greater than 2.27 Å. This has clear consequences for the mobility of the H atoms. Apart from the O-H bonds with all four types of H atoms, Hw and Hh are additionally fixed by hydrogen bonds. Hwa is relatively fixed by the tetrahedral orbital system of the water molecule; only Hha is relatively free. This would explain why the isotropic displacement parameters of Hw, Hwa, and Hh are approximately equal, while that of Hha is approximately twice as large. It is possible that Hha is, in fact, split between two slightly different positions, but the X-ray data do not allow this to be shown definitely. From the difference-Fourier synthesis we assume a splitting essentially in the **bc** plane. The X-ray data at 215 K alone do not allow a distinction to be made between static and dynamic disorder of the Hha atom.

Meyer et al. (2001) recently published a detailed investigation into the temperature evolution of structural changes in *deuterated* lawsonite, using high-resolution, time-of-flight neutron powder diffraction data between 2 and 500 K. Their structure data allow us to compare the orientations of the deuterium-bearing components in the **bc** plane at 11 different temperatures. Figure 5 shows the rotation angles of the D_2O molecules and OD groups out of or with respect to the **ab** plane in *deuterated* lawsonite as a function of temperature (filled symbols). For comparison, the values for *natural* lawsonite at 215 K (this study) are also included (open symbols). The rotation angle of the D_2O or H_2O molecule can, in principle, be used to study the temperature evolution of the microscopic order parameter in lawsonite, but only structure data at say 20–30 well-chosen temperatures would allow us to study both low-temperature phase transitions and the crossover behavior. A detailed strain analysis of deuterated and hydrogenated lawsonite (Carpenter et al. 2003) shows that replacing H by D causes the *Pmcn-P*2_1*cn* transition point (T_2) to shift by ~27 K while the *Cmcm-Pmcn* transition point (T_1) remains the same within ±2 K. Contrary to the type **B** X-ray intensities, the strain data show a crossover anomaly so subtle that it is only noticable by plotting the strains vs. each other. Replacing H by D causes the anomaly to shift from ~225 to ~250 K. The strains of the natural (hydrogenated) sample are consistently smaller than those of the deuterated sample. This is in agreement with the fact that the rotation angles of the hydrogen-bearing components are consistently smaller than those of the deuterium-bearing components. The difference is particularly striking between the O4-Hha and the O4-Dda groups. These observations imply that the structural rearrangements due to the low-temperature phase transitions are altogether smaller for the natural sample than for the deuterated sample. In addition, a comparison of the structures of deuterated and natural lawsonite at similar temperatures (natural sample at 215 K, deuterated sample at 225 K) shows that Dda is more fixed by "hydrogen" bonds than Hha (hence the smaller isotropic displacement parameter), while Dwa, on the other hand, appears to be much more loosely fixed than Hwa.

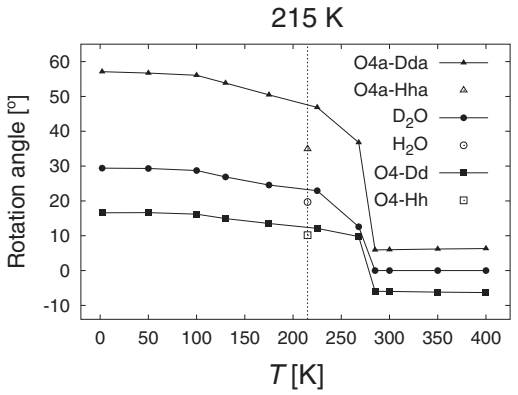

FIGURE 5. Filled symbols: rotation angles of the D_2O molecules and OD groups (O4-Dd, O4a-Dda) in deuterated lawsonite as function of temperature (Meyer et al. 2001). Open symbols: rotation angles of the H_2O molecules and OH groups (O4-Hh, O4a-Hha) in natural (hydrogenated) lawsonite at 215 K (this study). The rotation angle is defined here as the angle between the vector component of the electric dipole moment of the molecule/group in the **bc** plane and the basis vector **b**.

Elastic measurements

Figure 6 shows the temperature dependence of the elastic constants C_{ii} (i = 1–6), obtained experimentally in the temperature range 102–723 K. The data below 294 K (solid lines) were obtained on stepwise cooling (rate: 20 Kh^{-1}), using the continuous-wave resonance (cw) technique. The data from 294 K upward (filled circles) are from Brillouin spectroscopic measurements (Schilling et al. 2003). The elastic constants C_{ii} obtained from the cw measurements were renormalized with respect to the room-temperature values of C_{ii} based on the Brillouin measurements, assuming that the absolute values of the Brillouin data are more reliable than those of the cw data. The absolute error of the Brillouin data is supposed to be less than 1%, while that of the cw data should be less than 5%. Actually, the absolute values of the cw data turned out to be systematically lower by 10–20% than those of the Brillouin data. By contrast, the cw and pulse-echo data of the calibrant, C_{11} and C_{44} of pure $KMnF_3$, differ by less than 1.5%. While the synthesized calibrant samples were cut from a nearly perfect single crystal, the natural lawsonite sample used for the cw measurements had a lot of microcracks, which typically lower the absolute value of the elastic constant. We therefore conclude that the main contribution to the lowering of the absolute values of the elastic constants using the cw technique must be due to the imperfection of the lawsonite crystal. The effect of dispersion should be much smaller and can be neglected in this context, as can be seen from the good agreement between the cw and pulse-echo data of the calibrant. Contrary to the absolute error, the relative error of the cw data

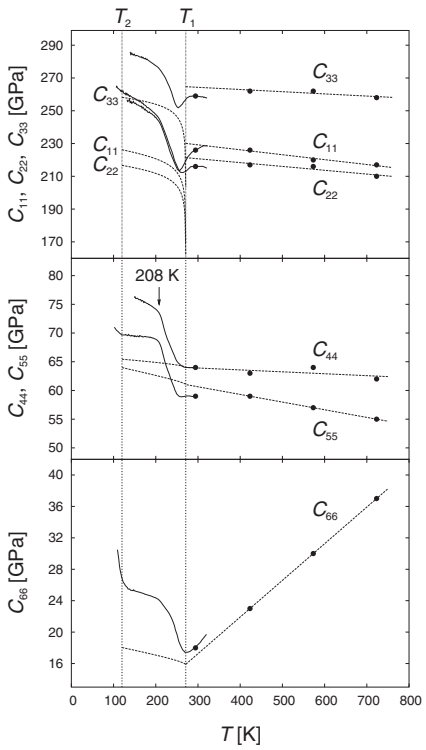

FIGURE 6. Temperature dependence of the experimental elastic constants C_{ii} (i = 1–6), obtained with the cw technique (solid lines) and from Brillouin data (filled circles), and of the predicted elastic constants C_{ii} (i = 1–6) (dashed lines), assuming a tricritical *Cmcm-Pmcn* transition driven by a single order parameter (Carpenter et al. 2003). The experimental value of C_{11} lies between that of C_{22} and C_{33} throughout the temperature range examined, even though C_{11} and C_{22} come remarkably close to each other in the region 208–256 K.

is supposed to be less than 1% and is essentially not affected by microcracks, so that the renormalization procedure, as outlined above, should lead to quite reliable results.

In addition to the experimental data, Figure 6 presents the temperature evolution of the three elastic constants C_{11}, C_{22}, and C_{33} (Eqs. 4 and 6) and of C_{44}, C_{55}, and C_{66} (Eq. 5) for the *Cmcm-Pmcn* transition, as predicted by Carpenter et al. (2003). The calculations are based on the assumption of a simple tricritical transition driven by a single order parameter, with Landau coefficients from calorimetric measurements (Martín-Olalla et al. 2001) and coupling coefficients from strain data (Carpenter et al. 2003), as given in Table 5. The coupling coefficients λ_4, λ_5, and λ_6, however, cannot be predicted from the model. Instead, they were estimated as the arithmetic average of $|\lambda_1|$, λ_2, and λ_3, in order to be able to predict the behavior of C_{44}, C_{55}, and C_{66} below T_1 at least qualitatively. This appears to be a reasonable estimate given that all six coupling coefficients should be of the same order of magnitude and $|\lambda_1|$, λ_2, and λ_3 have very similar values. In addition, λ_4, λ_5, and λ_6 are expected to be positive. The temperature evolution of the bare elastic constant C_{ii}^0 (i = 1–5) was estimated by linear extrapolation of the three Brillouin data points above 350 K, excluding the room-temperature value which is likely to be affected by the influence of elastic

TABLE 5. Values of the coefficients in Equation 2, from Martín-Olalla et al. (2001) and Carpenter et al. (2003) to calculate changes in the elastic constants due to the *Cmcm-Pmcn* transition

λ_1 = –0.710 GPa	a = 0.000226 GPa/K
λ_2 = 0.702 GPa	b^* = 0 GPa
λ_3 = 0.716 GPa	b = 0.0167 GPa
$\lambda_4 \approx \lambda_5 \approx \lambda_6 \approx$ 0.709GPa	c = 0.0786 GPa
T_c = 271 K	

Note: λ_4, λ_5, and λ_6 are only roughly estimated as the arithmetic average of $|\lambda_1|$, λ_2, and λ_3.

softening ahead of the *Cmcm-Pmcn* transition. In the case of C_{66}^0 the situation is more complicated. An extrapolation of the three Brillouin data points above 350 K down to low temperatures does not represent the pure bare elastic constant C_{66}^0. If it did, its slope would be slightly negative and of the same order of magnitude as that of the bare elastic constants C_{44}^0 and C_{55}^0. Instead, the positive slope of C_{66}^0 in the *Cmcm* phase indicates an orthorhombic-monoclinic phase transition at very low temperatures. In the following, we assume that this phase transition is essentially suppressed by the *Cmcm-Pmcn* transition. Only in this way can the overall pattern of behavior of C_{66} in the range T_1-T_2 be similar to that of C_{44} and C_{55}, which is reasonable. In order to roughly estimate the temperature evolution of C_{66}^0, excluding the effect of the orthorhombic-monoclinic transition below T_1, and thus to predict the temperature evolution of C_{66} between T_1 and T_2, we used the arithmetic average of the slopes of C_{44}^0 and C_{55}^0 for determining C_{66}^0.

The experimental data of the elastic constants are obviously in striking contrast to the predicted behavior, implying that a simple model, based on a tricritical transition driven by a single order parameter, is not adequate to describe the *Cmcm-Pmcn* transition—in contradiction to recently published strain, birefringence, and IR data. We conclude that the prediction of the elastic properties of lawsonite through the two low-temperature phase transitions by Carpenter et al. (2003), which is otherwise in full agreement with the strain, birefringence, and IR data, captures only the contribution of the displacive component involved in the *Cmcm-Pmcn* transition. In the light of these findings, a comparison of the experimental elastic data with the prediction is still useful to separate the influence of the displacive component from other possible effects, such as the suppression of the orthorhombic-monoclinic transition around T_1 as well as pretransitional and dynamic or kinetic effects in connection with the *Cmcm-Pmcn* transition. From the comparison it is also easy to see that below 208 K the observed overall pattern of behavior of the *Cmcm-Pmcn* transition follows the prediction by Carpenter et al. (2003) for a classical tricritical transition driven by a single order parameter, and below T_2 the influence of the *Pmcn-P*2_1*cn* transition is also consistent with the prediction of a second order transition.

In detail, the five experimental elastic constants C_{ii} (i = 1, 2, 3, 4, 5) vary fairly linearly above 350 K with only a slightly negative slope, as would be expected for the elastic constants of most silicates. The situation is different in the case of C_{66}, which varies linearly, but with a strongly positive slope. The influence of the *Cmcm-Pmcn* transition on C_{66} is quite similar in form to the variations shown by the other elastic constants, which is consistent with a suppression of the orthorhombic-monoclinic transition around T_1. Each of C_{11}, C_{22}, and C_{33} shows a minimum

around ~257 K which coincides with a break in slope for C_{44} and C_{55}. Surprisingly, there is no discrete anomaly around T_1 and the elastic softening seems to be smeared over a large temperature range far below the transition temperature. Undeniably, most of the elastic constants examined show an anomaly in terms of a kink around ~208 K (C_{11}, C_{22}, C_{44}, and C_{55}). The anomaly at this temperature is least pronounced for C_{33} and C_{66}.

Only the temperature evolution of C_{11}, C_{55}, and C_{66} could be determined below T_2, with a lower temperature limit between 110 and 102 K. In addition, Landau coefficients and coupling parameters are not yet available for the *Pmcn-P*2_1*cn* transition. It follows that little can be said about the effect of this transition on the elastic properties, other than that its influence on C_{11} seems to be very small, while it is more significant in the case of C_{55} and C_{66}. Assuming a base line given by the elastic constant of the *Pmcn* phase extrapolated into the stability region of the *P*2_1*cn* phase, the excess values of C_{55} and C_{66} appear to increase linearly on cooling below T_2, which is in good agreement with Equations 5 and 8, assuming that order-parameter saturation can be neglected. Like the intensities of type **C** reflections, the variations of the elastic constants are also consistent with a simple second-order transition around T_2. In addition, C_{66} appears to show pretransitional effects up to 20 K above T_2.

Discussion

The temperature dependence of physical properties such as specific heat (Martín-Olalla et al. 2001), birefringence, lattice parameters, and IR line widths (Meyer et al. 2000, 2001; Carpenter et al. 2003; Sondergeld et al. 2000a, 2000b) essentially confirm the tricritical nature of the *Cmcm-Pmcn* transition in lawsonite. The birefringence and strain data reveal significant pretransitional effects above T_1. At lower temperatures order parameter saturation also has to be taken into account. None of these physical properties, however, give hints of any significant complications in the evolution of the order parameter below T_1. These observations are in striking contrast with the intensity evolution of critical X-ray reflections in natural lawsonite. As can be seen from Figure 3, the square of the averaged and normalized intensity I_B of ten of the strongest type **B** reflections shows a significant kink around ~222 K. Given that the intensity I_B varies as $I_B \propto Q_1^2$, there must be a kink in the order parameter evolution. The existence of another phase transition between T_1 and T_2 can probably be ruled out and a crossover region between temperature intervals with different order parameter behavior seems the most likely explanation. The fact that properties which are directly coupled with the order parameter, such as strain, birefingence, and IR line width, do not show clear changes in trend around the crossover temperature, might be ascribed to uncertainties in the estimation of the relevant base lines. Superlattice intensities give the variation of the order parameter more directly, as they are zero, by definition, in the high-symmetry phase. In addition, the strength of coupling with the order parameter differs between these properties. Carpenter et al. (2003) mention changes in trend of the strain evolution around ~250 K in deuterated, and around ~225 K in natural lawsonite samples, respectively, but the effect appears to be very small. Elastic constants differ from the other properties in that they depend on the second derivative of the free energy rather than simply reflecting the equilibrium evolution of the order parameter. They are therefore expected to be particularly sensitive to the influence of phase transitions (e.g., Carpenter and Salje 1998).

The elastic behavior of lawsonite can be subdivided into several distinct temperature intervals. In the stability field of the *Cmcm* phase, the elastic constants C_{ii} ($i = 1, 2, 3, 4, 5$) evolve in a normal manner, reflecting mainly the effects of thermal expansion. C_{66}, by contrast, softens with falling temperature and extrapolates to zero at ~–70 K. Clearly C_{66} does not reach zero as a function of temperature, but it might do so as a function of pressure. The condition "$C_{66} \rightarrow 0$" would lead to an orthorhombic $\rightarrow$ monoclinic transition, as has recently been reported at 9.5 GPa by Boffa Ballaran and Angel (2003) and Daniel et al. (2000) on applying pressure to lawsonite. This ferroelastic transition appears to be suppressed by the *Cmcm-Pmcn* transition and should thus be unrelated to the proton ordering processes below T_1. Ahead of the *Cmcm-Pmcn* transition there is some distinct softening of C_{11}, C_{22}, and C_{33}. This could be due to the effects of thermal fluctuations, in the usual way. Between ~270 and ~256 K C_{11}, C_{22}, and C_{33} all soften, but they do not show the break in slope or large discontinuity expected for a classical tricritical transition with one order parameter. Between ~256 and ~208 K all the elastic constants stiffen, but without following the simple behavior predicted for a one-component order parameter. The break in slope at ~208 K is not far from the break in slope (at ~222 K) observed in the intensities of superlattice reflections. From ~208 to ~120 K the elastic constants all continue to stiffen. Actually, as can be seen from Figure 6, the temperature evolution of all six experimental elastic constants C_{ii} ($i = 1, 2, 3, 4, 5, 6$) below 208 K follows the overall pattern of behavior that is predicted for a tricritical *Cmcm-Pmcn* transition driven by a single order parameter. The effect of the crossover seems to be, consistently, an increase of the elastic constant and a modification of the coupling coefficient, but the order of magnitude remains the same in both cases. The pattern of behavior below 208 K, both experimentally and predicted, is also consistent with a suppression of the monoclinic-orthorhombic phase transition around T_1. At 120 K the onset of anomalies associated with the *Pmcn-P*2_1*cn* transition is observed. The contributions of the two ordering processes below T_2 seem to be additive (see the curves of C_{55} and C_{66}). In other words, a coupling of the two order parameters Q_1 and Q_2 can be neglected in this context.

There appear to be two possible additional aspects of the phase transition at T_1 which need to be added to any model. A classical one-component order parameter model is clearly inadequate. One possibility is that there are two order parameters with the same symmetry, one relating to proton ordering and the second to displacements of the framework atoms. If these are not linearly dependent on each other, crossover behavior of the type which appears to take place at ~208 K could occur. General cases for this type of behavior are described by Devarajan and Salje (1986), for example. Alternatively, there may be some involvement of dynamical effects, particularly in relation to the proton ordering. This could be responsible for the tail in strain and heat capacity above T_1 and for the smearing out of the elastic constants through the transition point. Further work is in progress to investigate these possibilities in detail.

ACKNOWLEDGMENTS

The authors thank A. Pring from the University of Adelaide, Australia, and E. Libowitzky for supplying the samples used in this study. Thanks also go to C. Hejny for contributing to the data collection of the critical X-ray reflections and, last but not least, to H. Kabelka for fruitful discussions. This project was supported by the EU TMR Network on Mineral Transformations (ERB-FMRX-CT97-0108).

REFERENCES CITED

Boffa Ballaran, T. and Angel, R.J. (2003) Equation of state and high-pressure phase transitions in lawsonite. European Journal of Mineralogy, 15, 241–246.

Bolef, D.I. and Menes, M. (1960) Measurement of elastic constants of RbBr, RbI, CsBr and CsI by an ultrasonic cw resonance technique. Journal of Applied Physics, 31, 1010–1017.

Carpenter, M.A. and Salje, E.K.H. (1998) Elastic anomalies in minerals due to structural phase transitions. European Journal of Mineralogy, 10, 693–812.

Carpenter, M.A., Meyer, H.-W., Sondergeld, P., Marion, S., and Knight, K.S. (2003) Spontaneous strain variations through the low-temperature phase transitions of deuterated lawsonite. American Mineralogist, 88, 534–546.

Daniel, I., Fiquet, G., Gillet, P., Schmidt, M.W., and Hanfland, M. (2000) High-pressure behaviour of lawsonite: A phase transition at 8.6 GPa. European Journal of Mineralogy, 12, 721–733.

Devarajan, V. and Salje, E.K.H. (1986) Phase transitions in langbeinites II: Raman spectroscopic investigations of $K_2Cd_2(SO4)_3$. Physics and Chemistry of Minerals, 13, 25–30.

Gibaud, A., Shapiro, S.M., Nouet, J., and You, H. (1991) Phase diagram of $KMn_{1-x}Ca_xF_3$ ($x < 0.05$) determined by high-resolution X-ray scattering. Physical Review B, 44, 2437–2443.

Hayward, S.A., Burriel, R., Marion, S., Meyer, H.-W., and Carpenter, M.A. (2002) Kinetic effects associated with the low-temperature phase transitions in lawsonite. European Journal of Mineralogy, 14, 1145–1153.

Lager, G.A., Libowitzky, E., and Schultz, A.J. (1998) Neutron diffraction study of the low-temperature phase transitions in lawsonite. Proceedings of the 17th General Meeting of the International Mineralogical Association, Toronto, A99.

Libowitzky, E. and Armbruster, T. (1995) Low-temperature phase transitions and the role of hydrogen bonds in lawsonite. American Mineralogist, 80, 1277–1285.

——— (1996) Lawsonite-type phase transitions in hennomartinite, $SrMn_2[Si_2O_7](OH)_2 \cdot H_2O$. American Mineralogist, 81, 9–18.

Martín-Olalla, J.-M., Hayward, S.A., Meyer, H.-W., Ramos, S., del Cerro, J., and Carpenter, M.A. (2001) Phase transitions in lawsonite: A calorimetric study. European Journal of Mineralogy, 13, 5–14.

Meyer, H.-W., Carpenter, M.A., Graeme-Barber, A., Sondergeld, P., and Schranz, W. (2000) Local and macroscopic order parameter variations associated with low-temperature phase transitions in lawsonite, $CaAl_2Si_2O_7(OH)_2 \cdot H_2O$. European Journal of Mineralogy, 12, 1139–1150.

Meyer, H.-W., Marion, S., Sondergeld, P., Carpenter, M.A., Knight, K.S., Redfern, S.A.T., and Dove, M.T. (2001) Displacive components of the low-temperature phase transitions in lawsonite. American Mineralogist, 86, 566–577.

Pawley, A.R. (1994) The pressure and temperature stability limits of lawsonite: Implications for H_2O recycling in subduction zones. Contributions to Mineralogy and Petrology, 118, 99–108.

Schilling, F.R., Sinogeikin, S.V., and Bass, J.D. (2003) Single-crystal elastic properties of lawsonite and their variation with temperature. Physics of the Earth and Planetary Interiors, 136, 107–118.

Sheldrick, G.M. (1997) SHELX-97. Program package for crystal structure determination. University of Göttingen, Germany.

Slonczewski, J.C., and Thomas, H. (1970) Interaction of elastic strain with the structural transition of strontium titanate. Physical Review B, 1, 3599–3608.

Sondergeld, P., Schranz, W., Kityk, A.V., Carpenter, M.A., and Libowitzky, E. (2000a) Ordering behavior of the mineral lawsonite. Phase Transitions, 71, 189–203.

Sondergeld, P., Schranz, W., Tröster, A., Carpenter, M.A., Libowitzky, E., and Kityk, A.V. (2000b) Optical, elastic, and dielectric studies of the phase transitions in lawsonite. Physical Review B, 62, 6143–6147.

MANUSCRIPT RECEIVED JANUARY 10, 2003
MANUSCRIPT ACCEPTED JULY 23, 2004
MANUSCRIPT HANDLED BY KARSTEN KNORR